AD_____

AWARD NUMBER DAMD17-97-1-7300

TITLE: Computer Simulation Of X-Ray Capillary Optics For Digital Mammography

PRINCIPAL INVESTIGATOR: Hui Wang
Dr. Carolyn MacDonald

CONTRACTING ORGANIZATION: State University of New York at Albany
Albany, New York 12222

REPORT DATE: September 1999

TYPE OF REPORT: Annual

PREPARED FOR: U.S. Army Medical Research and Materiel Command
Fort Detrick, Maryland 21702-5012

REPORT DOCUMENTATION PAGE

Form Approved
OMB No. 0704-0188

1. AGENCY USE ONLY *(Leave blank)*	2. REPORT DATE	3. REPORT TYPE AND DATES COVERED
	September 1999	Annual (1 Sep 98 - 31 Aug 99)

4. TITLE AND SUBTITLE
Computer Simulation of X-Ray Capillary Optics for Digital Mammography

5. FUNDING NUMBERS
DAMD17-97-1-7300

6. AUTHOR(S)
Hui Wang
Dr. Carolyn MacDonald

7. PERFORMING ORGANIZATION NAME(S) AND ADDRESS(ES)
State University of New York at Albany
Albany, New York 12222

8. PERFORMING ORGANIZATION REPORT NUMBER

9. SPONSORING / MONITORING AGENCY NAME(S) AND ADDRESS(ES)
U.S. Army Medical Research and Materiel Command
Fort Detrick, Maryland 21702-5012

10. SPONSORING / MONITORING AGENCY REPORT NUMBER

11. SUPPLEMENTARY NOTES

12a. DISTRIBUTION / AVAILABILITY STATEMENT
Approved for public release; distribution unlimited

12b. DISTRIBUTION CODE

13. ABSTRACT *(Maximum 200 words)*

The objective of this proposal is to develop a digital mammographic imaging system with high contrast, good resolution, and low patient dose. A new technology, polycapillary optics, has been shown to produce clearer images by increasing contrast and resolution. A number of prototype systems are being studied: borosilicate and leaded glass fibers, collimating and monolithic focusing lenses. A number of fibers have been measured and simulated in the energy range 10- 80keV. Short lead glass optics seem promising for scatter rejection. A long focal length collimating lens has transmission close to 45% at mammographic energies. The monolithic focusing lens with focal distance is 50 cm has transmission of 21% at 20 keV.

14. SUBJECT TERMS
Breast Cancer

15. NUMBER OF PAGES
23

16. PRICE CODE

17. SECURITY CLASSIFICATION OF REPORT	18. SECURITY CLASSIFICATION OF THIS PAGE	19. SECURITY CLASSIFICATION OF ABSTRACT	20. LIMITATION OF ABSTRACT
Unclassified	Unclassified	Unclassified	Unlimited

FOREWORD

Opinions, interpretations, conclusions and recommendations are those of the author and are not necessarily endorsed by the U.S. Army.

d Where copyrighted material is quoted, permission has been obtained to use such material.

d Where material from documents designated for limited distribution is quoted, permission has been obtained to use the material.

d Citations of commercial organizations and trade names in this report do not constitute an official Department of Army endorsement or approval of the products or services of these organizations.

____ In conducting research using animals, the investigator(s) adhered to the "Guide for the Care and Use of Laboratory Animals," prepared by the Committee on Care and use of Laboratory Animals of the Institute of Laboratory Resources, national Research Council (NIH Publication No. 86-23, Revised 1985).

____ For the protection of human subjects, the investigator(s) adhered to policies of applicable Federal Law 45 CFR 46.

____ In conducting research utilizing recombinant DNA technology, the investigator(s) adhered to current guidelines promulgated by the National Institutes of Health.

____ In the conduct of research utilizing recombinant DNA, the investigator(s) adhered to the NIH Guidelines for Research Involving Recombinant DNA Molecules.

____ In the conduct of research involving hazardous organisms, the investigator(s) adhered to the CDC-NIH Guide for Biosafety in Microbiological and Biomedical Laboratories.

PI - Signature

9/30/99
Date

Table of Contents

1. Introduction

1.A Background:

Each year about 186,000 women contract breast cancer, of whom 46,000 will die of it. Breast cancer is the leading cause of cancer deaths amongst American women aged 35 to 50 and also has the highest cancer mortality rate for younger women. Mammography is most widely used modality for early detection of breast cancer. The detection of tiny carcinomas and low contrast tissue is essential for mammography to reduce the mortality rate[1, 2]. It has been shown that about 20% of detectable cancers are overlooked or misdiagnosed on first detection. We obviously need a major improvement in the quality of mammograghic imaging. Using an innovative new technology x-ray optics to improve system resolution, enhance contrast and reduce dosage will increase the effectiveness of this proven screening modality, with a direct impact on mortality.

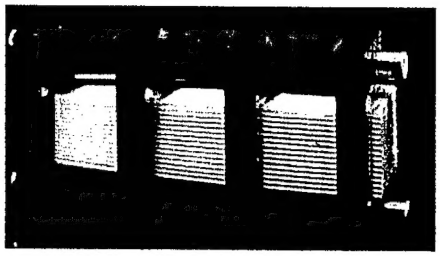

Figure 1 Complete optic constructed by configuring fibers through metal grids.

1.B Benefits of digital mammography

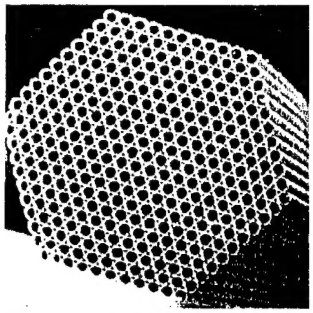

Figure 2 Cross section of polycapillary fiber. 0.5 mm in diameter. SEM photo.

Conventional film screen mammography suffers from limited dynamic range and film granularity, which can reduce the sensitivity to detect microcalcifications. The primary theoretical limitations of mammography are the system resolution, which determines the minimum size of the detectable malignancy, and the need to expose the patient to ionizing radiation. Using innovative new technology -- polycapillary optics -- to improve system resolution and reduce required dose will increase the effectiveness of this proven screening modality, with a direct and immediate impact on mortality. By matching polycapillary optics to digital detectors, we can develop direct digital mammographic systems which can avail themselves of the advantages of digital processing, including improved image contrast and resolution at reduced radiation dose. In practice, mammographic imaging is often limited by quality assurance issues, which can also be favorably addressed by digital processing. Digital detection can provide high dynamic range which, in addition to improving contrast, greatly increases the tolerance of the final image to under or over exposure. Digital images can be enhanced and are amenable to computer-aided diagnosis. Finally, digital images can also be transported quickly for skilled consultations.

1.C What capillary x-ray optics can do

Capillary optics, consisting of arrays of hollow glass tubes, is a relatively new technology for controlling X-ray beams. X-rays incident on the interior of the glass tubes at small angles are guided down the tubes by total external reflection. Arrays of curved/tapered capillaries can be used to focus, collimate and filter X-ray radiation[3,4,5,6,7]. Such arrays are manufactured by stringing hollow glass polycapillaries through metal grids (as in Figure 1) or as a monolithic optic.

The use of Kumakhov capillary optics in place of conventional scatter reduction grids in a mammographic system has significant potential to provide improved resolution, increased contrast enhancement and reduced dose in mammographic imaging. The optics can also be used to mate the radiographic image with a digital detector by appropriate choice of demagnification and separation to discrete chips. In addition, a pre-patient optic could be employed to increase the available intensity in a fan beam relative to simple slot collimating.

The fibers in this research varied from 0.3 mm to 4 mm in outer diameter, with channel sizes (the diameters of the holes within the fibers) ranging from 4 to 22 μm, as shown in Table 1 in section 2.E. Open area in the table refers to the fraction of the front face of the fiber which is open channels, as opposed to glass walls. No fiber can have a transmission that is greater than the open area.

X-ray beams can be bent, focused or collimated by a carefully curved polycapillary array. X-ray photon energies are much larger than the plasma frequencies of glasses, which are tens of electron volts. In this regime, the real part of the index of refraction of glass can be simply approximated by

$$n^2 = \frac{\varepsilon}{\varepsilon_o} \approx 1 - \frac{\omega_p^2}{\omega^2} \quad (1)$$

where n is the index of refraction, ε is the dielectric constant of the glass, ω is the photon frequency, ω_p is the plasma frequency of the material, and ε_0 is the dielectric constant for vacuum.

The plasma frequency ω_p for glass is small compared to the photon frequency, so that n is slightly less than unity. Therefore, x rays traveling in vacuum or air can be totally externally reflected from smooth glass surfaces. The maximum angle between the x-ray beam and glass surface for total reflection, θ_c, is approximately

$$\theta_c = \frac{30}{E} \text{ mrad}, \quad (2)$$

where E is the photon energy in keV. The higher the energy of photon, the smaller is the critical angle. For this reason, profile errors that change the angle of incidence are more detrimental at high energies.

1.D Numerical simulations

To evaluate the experimental performance of capillaries and optics, and to design capillary optics, it is necessary to be able to predict theoretical behavior for complex geometries. Extensive modeling programs describing the propagation of x-rays along capillaries and optics are being developed. These modeling programs provide essential information on the transmission efficiency and divergence of capillary optics, and are being used to simulate the performance of the optics by obtaining the following outputs: transmission efficiency, exit divergence, output uniformity, and transmission as a function of entrance angle.

The models for these simulation programs are based on Monte Carlo simulations of simple geometrical optics. The simulations randomly generate millions of x-ray photons from a particular location and solid angle, and then trace them through the optics using reflection theory and classic mechanics. The necessary confidence in the simulations is being built by comparing the results of the modeling program with experimental data.

For single fibers, the computational speed is greatly enhanced by a reduction to two dimensions by projecting the trajectory onto the local fiber cross-section.[8] Reflections are computed from standard tables.[9]

1.E Purpose

The purpose of this project is to contribute to an ongoing effort to use the new innovative technologies in X-ray optics to develop a digital mammographic imaging system with high resolution and contrast by extending the capabilities of the computer simulation. Enhanced computer simulations are critical because manufacturing large polycapillary optics is difficult, expensive and time-consuming, and simulation is a good design tool to predict the performance of the optics and make it clear how all the different parameters work together and impact the resultant transmission, resolution and contrast.

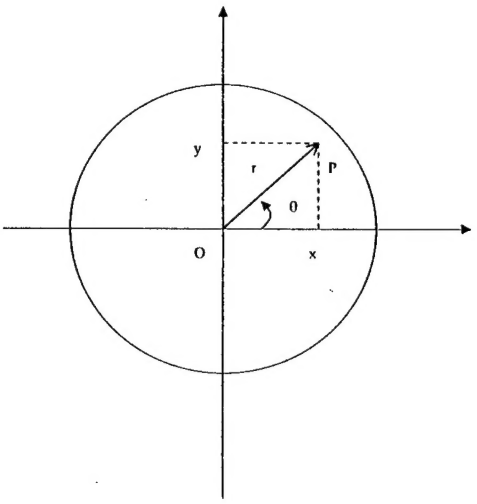

Figure 3. The generation of a random point (of a photon) in a circle.

1.F Technical objectives

The specific aims of this traineeship are:

- to simulate and measure trial optic setups, to compare the simulated results with experimental data and to determine the best design for building the best direct digital mammographic system;
- to further the author's knowledge about the mammographic systems and to promote a future career in this field.

2. Body: Methods and Results

2.A Introduction to profile and surface defect corrections

Real glass surfaces are not perfect. In addition to absorption, there is roughness, which has short wavelengths, of the order of microns or less, waviness, which has longer wavelength, and bending, which has wavelength longer than the length of the capillary. Bending is described by the radius of curvature of the fiber, R in Table 1. Waviness results in the channel wall being tilted with respect to the axis of the fiber, and therefore changes the angle of incidence. It is described in terms of a distribution of tilt angles. Surface roughness produces both diffuse scattering, for which the reflected angle can be either larger or smaller than the corresponding incident angle, and transmission into the glass. The roughness correction[10] used in previous simulations[11] is described in terms of a roughness height, z and a correlation length, s.

2.B Current progress

To provide a framework for assessing the results of the first year of the project, the original statement of work for the full three-year project is reproduced below.

Proposed Statement Of Work

Task 1 Developing and testing the simulation software. (months 1-18)

Task 2: Perform experiment and geometric simulations on pre-patient collimating optic at a wide range of energies (month 19-23)

2.1 Measure transmission as a function of x-ray energy.

2.2 Measure transmission uniformity.
2.3 Measure dependence of transmission on x-ray entrance angle.
2.4 Perform geometric simulation on transmission spectra.

Task 3: Perform experiments on collimating optic at mammographic energies. (month 24-26)
3.1 Measure exit angle divergence.
3.2 Measure contrast enhancement.

Task 4: Perform experiments and geometric simulations on post-patient anti scatter optic. (month 27-30)
4.1 Measure central part and whole optics as a function of photon energy
4.2 Measure transmission uniformity
4.3 Measure dependence of transmission on x-ray entrance angle
4.4 Perform geometric simulation on transmission spectra

Task 5: Perform experiments on post- patient anti scatter optic at mammographic energies (month 31-33)
5.1 Measure transmission energy as a function of photon energy
5.2 Measure transmission uniformity
5.3 Measure transmission entrance angle dependence
5.4 Measure scatter fraction
5.5 Measure contrast enhancement
5.6 Measure uniformity of magnification factor

Task 6. Design assessment (month 34-36)

In the first year of this project, we developed and tested a more physical model and compared the simulation results for a variety of straight capillaries to measured data in the energy range from 10 to 80 keV. Using this analysis, the number of required parameters in this energy range, including 20 keV for mammography, is reduced from four to two, bending curvature and waviness. It was not found to be necessary to include roughness effects. Although, it took more than a year to develop this unexpected new model and perform its implementation for single fibers and lenses, it was worthwhile because we now have a more physical simulation model which increases the time efficiency for future modeling.

Sections 2C-2E are the comparison of the new model with the previous model and the comparison of their simulation results with the experimental data for borosilicate glass optics. Section 2F-2G presents new data and simulations applied during the second year to lead glass optics. During the second year the principal investigation was changed from Hui Wang to Cari.

2.C Improvement in generating x-ray photons

As shown in Figure 3, to produce a random point P in a circle, we can randomly generate either (r, θ) or (x, y). Previous simulations[11] used uniformly generated θ in the range (0, 2π) and r in the range (0, R), where R is the radius of the x-ray source, capillary channel or fiber input area. This work uniformly generated x and y coordinates, with the limitation $x^2 + y^2 < R^2$, which is closer to an isotropic distribution.

2.D Improvements in waviness correction model

Waviness of a capillary surface is oscillations with wavelengths shorter than the capillary length and longer than the wavelength of the roughness. The waviness effect is modeled as a random tilt of the glass wall, which results in a random change in the reflection angle on each bounce. If the random tilt angle is ϕ and the incident angle is θ, then the reflection angle with respect to the nominal surface will be $\theta+2\phi$, as shown in Figure 4. Previous simulations used a uniform distribution model; this work uses a tilt-corrected normal distribution to generate ϕ.

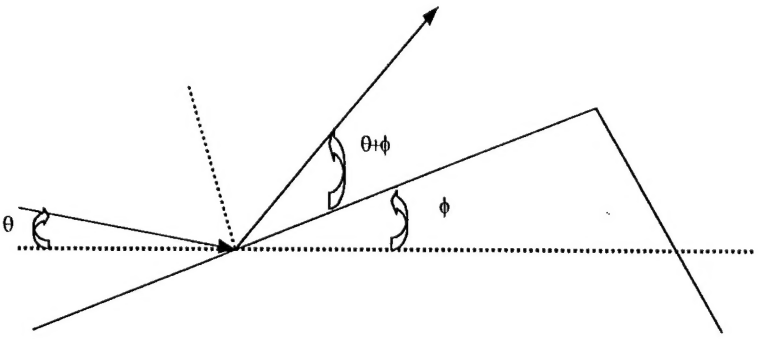

Figure 4. Scheme of an x-ray beam interactions with a randomly tilted surface.

2.D.1 Uniform distribution model

Previous simulations, referred here as Model M1, assumed a uniform distribution of 2ϕ from $-\Delta\theta_{max}$ to $\Delta\theta_{max}$ if $\theta \geq \Delta\theta_{max}$, or from $-\theta$ to $\Delta\theta_{max}$ if $\theta \leq \Delta\theta_{max}$. The maximum random tilt angle $\Delta\theta_{max}$ is the adjustable parameter which describes the amount of waviness of the capillary.

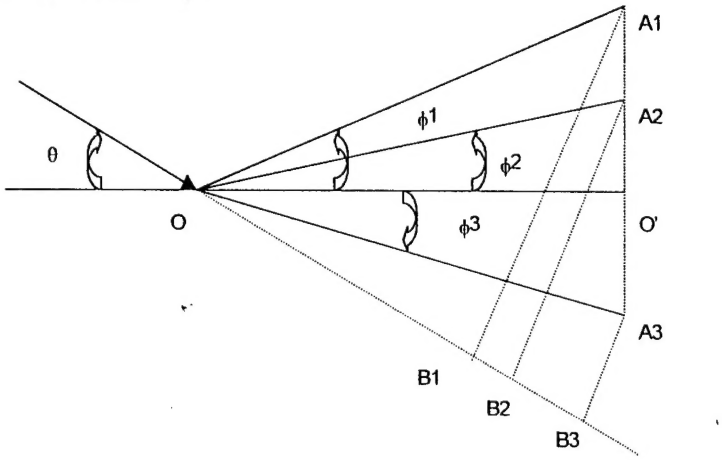

Figure 5. Three surfaces, OA_1, OA_2 and OA_3, with different tilt angles, ϕ_1, ϕ_2 and ϕ_3, respectively, from the nominal surface OO'. Here, $-\theta \leq \phi_3 \leq 0$, $OA_1*\cos\phi_1 = OA_2*\cos\phi_2 = OA_3*\cos\phi_3 = OO'$.

2.D.2 Tilt-corrected normal distribution model

2.D.2.1 Normal distribution

For this work, named as Model M2, it is assumed that these tilt angles, ϕ, are normally distributed in the range $(-\pi/2, \pi/2)$. with the mean value equal to zero. For high quality optics, the standard deviation of this normal distribution, σ, is much smaller than the critical angle, θ_c. The probability distribution of tilt angles, ϕ, is

$$G(\phi) = \frac{1}{\sigma\sqrt{2\pi}} e^{-\frac{\phi^2}{2\sigma^2}}. \qquad (3)$$

2.D.2.2 X-ray impact tilt correction

In this work, Model M2, consideration was taken of the fact that the surface tilt angle will affect the probability of x-ray impact on that surface. Taken to extremes, a surface region perpendicular to the beam is much more likely to intercept the beam than a surface region parallel to the beam. Figure 5 displays three surfaces, OA_1, OA_2 and OA_3, with different tilt angles, ϕ_1, ϕ_2 and ϕ_3, respectively, from the nominal surface OO'. The projections onto the nominal surface for the three surfaces are equal, $OA_1*\cos\phi_1 = OA_2*\cos\phi_2 = OA_3*\cos\phi_3 = OO'$. The probability of incidence of a parallel x-ray beam with

incident angle θ (with respect to the nominal surface OO') hitting these tilted surfaces is given by their corresponding perpendicular length A_jB_j (for j = 1, 2 or 3)

$$P_j \propto A_jB_j = OA_j \cdot \sin(\theta+\phi_j) = \frac{OO}{\cos\phi_j} \cdot \sin(\theta+\phi_j), \quad (4)$$

We call this the tilt-corrected probability distribution. The complete description of this distribution is

$$H(\phi) = \begin{cases} \frac{F\sin(\theta+\phi)}{\cos(\phi)}, & -\theta < \phi < \frac{\pi}{2} \\ 0, & -\frac{\pi}{2} < \phi \le -\theta \end{cases}, \quad (5)$$

where θ is the incident angle, ϕ is the tilt angle and F is a normalization constant.

2.D.2.3 Tilt-corrected normal distribution

Combining the normal distribution G(ϕ) with the tilt correction H(ϕ) gives ϕ for a certain incident angle θ as follows:

$$J(\phi) = \begin{cases} Ke^{\frac{-\phi^2}{2\sigma^2}} \cdot \frac{\sin(\theta+\phi)}{\cos\phi}, & -\theta < \phi < \frac{\pi}{2} \\ 0, & \frac{-\pi}{2} \le \phi \le -\theta \end{cases}, \quad (6)$$

where θ is the incident angle, ϕ is the tilt angle and K is a normalization constant.

Noting that

$$\frac{\sin(\theta+\phi)}{\cos\phi} = \sin\theta + \cos\theta \cdot \tan\phi \quad (7)$$

and that both the incident angle, θ, and the tilt angle, ϕ, are very much less than 40 mrad, we use the approximation

$$P(\phi) = \begin{cases} Ce^{\frac{-\phi^2}{2\sigma^2}} * (\theta+\phi), & -\theta < \phi < \frac{\pi}{2} \\ 0, & -\frac{\pi}{2} \le \phi \le -\theta \end{cases}, \quad (8)$$

where the normalization constant , C, is

$$C \approx \frac{1}{\sqrt{2\pi\theta\sigma + 2\sigma^2}}, \quad (9)$$

to speed the calculation. P(ϕ) is called the tilt-corrected normal distribution. In model M2, σ is the variable that describes the amount of waviness. Two examples of J(ϕ) and P(ϕ) are shown in Figure 6 and Figure 7.

Fiber Description						Model M1				Model M2	
Fiber #	Type	Outer Diame-ter mm	Channel Size μm	Open Area	Length mm	z nm	s μm	R m	$\Delta\theta_{max}$ mrad	R m	σ mrad
A	1	0.5	12	65%	105	0.7	6	105	0.4	60	0.225
C	3	0.75	22	50%	136	0.5	6	125	0.35	225	0.2
D	4	4	12	55%	130	0.8	6	110	0.285	139	0.125
E	5	0.3	4-5	55%	105	0.7	6	28	0.2	31	0.09
F	4	4	12	55%	130	0.8	6	90	0.45	90	0.18

Table 1 Parameters for best-fit simulations. R is the bending radius. For M1, $\Delta\theta_{max}$ is the amount of waviness, z is the roughness height and s is the roughness correlation length. For M2, σ is the standard deviation of the waviness.

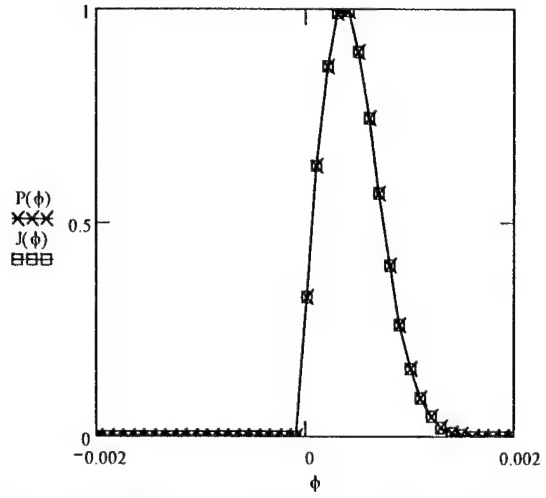

Figure 6. The probability distribution, J(ϕ), and its approximation, P(ϕ), versus tilt angle ϕ when incident angle θ = 0.0001 rad, standard deviation σ = 0.0004 rad. ϕ is in rad.

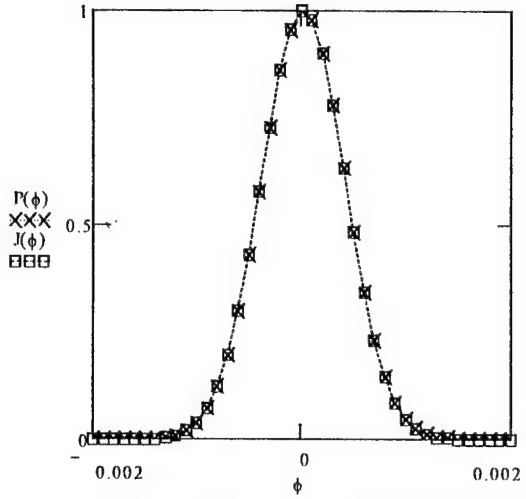

Figure 7. J(ϕ) and P(ϕ) versus tilt angle ϕ when incident angle θ = 0.009 rad, standard deviation σ = 0.0004 rad. ϕ is in rad.

2.E Results

Transmission of a number of different fibers measured previously[11] in the energy region 10-80 keV are shown in figures 8-18. The descriptions of these polycapillary fibers and their simulation parameters are shown in Table 1.

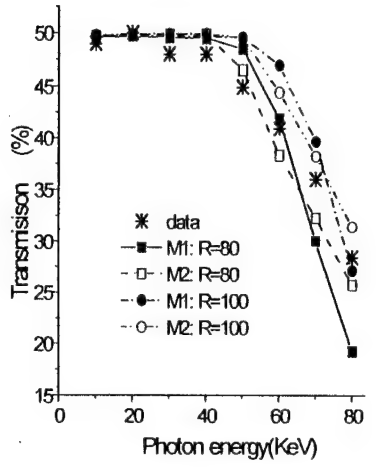

Figure 8 Transmission spectra for fiber C simulated with different bending curvature alone using models M1 and M2, compared with experimental data. This figure shows that the simulations with bending alone can not fit the data, and indicates that bending is not the only factor to cause the transmission drop.

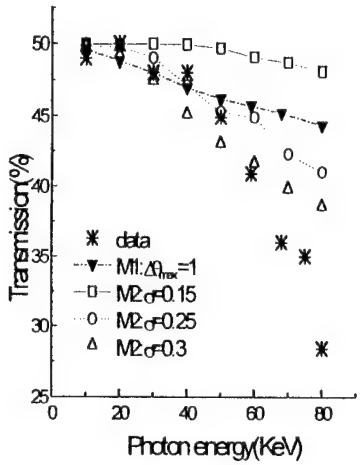

Figure 9 Simulations of transmission spectra for fiber C with only waviness compared with the experimental data. This figure shows the effects of waviness. It also shows simulations using waviness alone do not fit the data. The simulations do not include the roughness or bending correction.

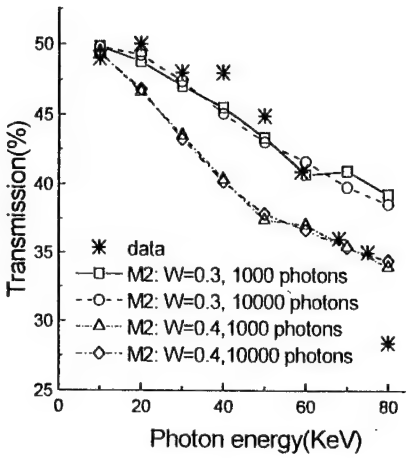

Figure 10 Simulations of transmission spectra with waviness correction using different numbers of photons, compared with the experimental data of fiber C. The figure shows that the simulation curves using 10000 photons are much smoother than those using 1000 photons because of the reduction in statistical fluctuation.

The experimental data and simulation results from the two simulations for a type 3 polycapillary, Fiber C, are compared first to demonstrate the fitting processes, to interpret the waviness and bending effects, and to understand the final results.

2.E.1 Bending effects

A slight bending can dramatically reduce the transmission of high-energy photons because of the small critical angle at high energies. Figure 8 shows a comparison between experimental data and simulations with different bend radii. The difference in the bending effect between M1 and M2 is due to the different algorithms used in generating x-ray photons as discussed in section 2.C. M1 assumes more photons hit the center of the fiber as well as the center of each channel. M2 generates photons uniformly across the channel, fiber and source.

For both models, a bend of R = 80 m reduces the transmission too much at high energies. Since any waviness or roughness correction, like the bending correction, will reduce the transmission, R must be larger than 80 meters. We set R_{min} = 80 m, which is useful in determining the best-fit parameters for the model M2.

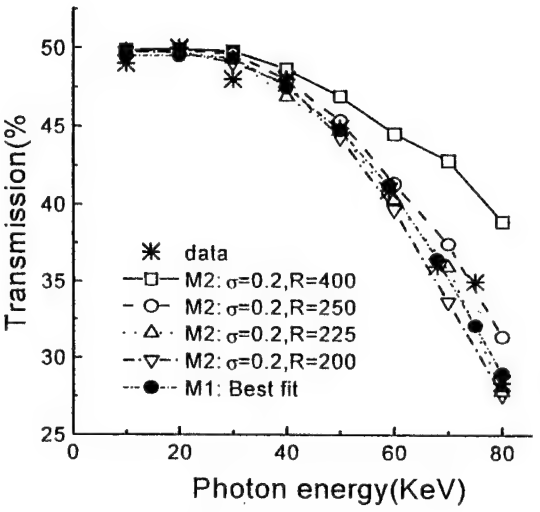

Figure 11. Simulated transmission spectra using model M2 with fixed waviness (σ=0.2 mrad) and different bending, compared with the experimental data. The simulation curves shown are just a few representative cases in the bisection process. For M2, the best-fit parameters are σ = 0.2 mrad and R = 225 m; for M1, they are z = 0.5 nm, s = 6 μm, $\Delta\theta_{max}$ = 0.35 mrad and R = 125 m.

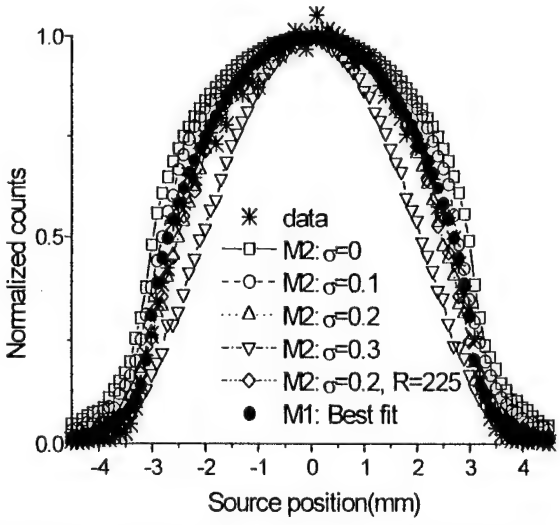

Figure 12. Simulations of source scan curve using model M2 with different waviness (σ) compared with the experimental data. The larger the waviness, the narrower the simulated scan curve. The simulation curves with the best fitting parameters of M1 and M2 obtained in Figure 11 are also shown in this figure for reference.

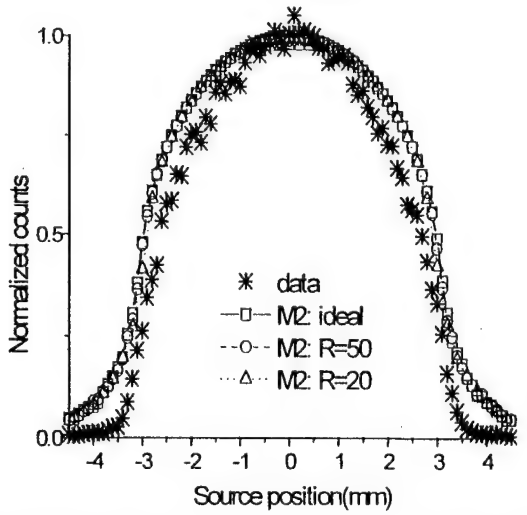

Figure 13 Simulations of source scan curves using model M2 with no waviness and different bending compared with the experimental data at 10 keV. The simulated scan curve does not become narrower even when the bending radius R = 20 m. The word "ideal" refers to a simulation with R=∞ and no waviness.

Clearly, bending alone cannot explain the experimental data, especially at low energies.

2.E.2 Waviness effects

To explain the data at energies from 20 to 60 keV, another correction is needed. Roughness does not have a major effect in this energy range[11]. Waviness is expected to be the major factor in this energy range.

Figure 9 shows that the transmission becomes lower for all the energies and the high-energy transmission drops faster with increasing σ gets larger. It also shows that waviness alone, like bending alone, can not explain the experimental data. In the simulation, σ = 0.3 mrad and 0.4 mrad are definitely over-correcting at low energies, so we can set 0.3 mrad as the maximum of σ (σ_{max}) for Fiber C. The waviness parameter Δθ for model M1 is larger than the parameter σ for model 2 because the tilt correction in model M2 makes it more probable that the x-ray will intersect the high angle surfaces.

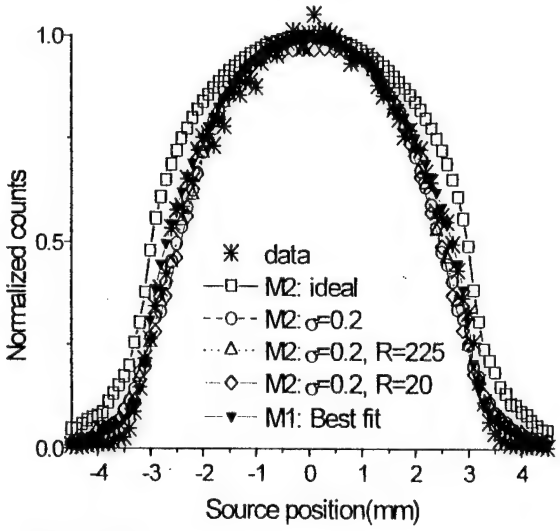

Figure 14 Simulations of source scan curves using model M2 with fixed waviness (σ = 0.2 mrad) and different bending compared with the experimental data. The simulated scan curve does not apparently change even when the bending radius R = 20 m. With and without the bending, simulations using σ =0.2 mrad fit the experimental data quite well.

The fluctuation of the simulation curve in Figure 9 when σ=0.25 mrad is mainly due to the relatively small number of photons, 1000, used in the simulation. Figure 10 shows the difference when the number of photons changes from 1000 to 10000.

Using a bisection algorithm with R_{min} and σ_{max}, R and σ were applied together and compared to the data to get the best fit parameters, as shown in Figure 11. The best fit parameters for fiber C using model M2 are R = 225 m and σ = 0.2 mrad.

2.E.3 Verification using the source scan curves

Figure 12 shows the source scan curve, that is transmission as a function of lateral source displacement, and simulation results, for increasing waviness for Fiber C at 10 keV. The simulated source scan slowly becomes narrower when σ gets larger, however that change is too small to be used to determine σ. *Figure 13* displays simulations for Fiber C at 10 keV with different R and no waviness. *Figure 14* shows the effect of different R with a fixed σ. From these two figures, it is apparent that changing R from 20 meters to infinity does not have any visible effect on the fitting curve. Therefore, we can not use the simulations of the source scan curves to determine either σ or R, but they can be used to verify σ.

For Fiber C, as shown for 10 keV in Figure 12, at higher energies in Figure 15, and as a function of energy in Figure 11, the simulation curve of σ=0.2 mrad fits the experiment data very well with one fewer fitting parameter than the best fit of M1.

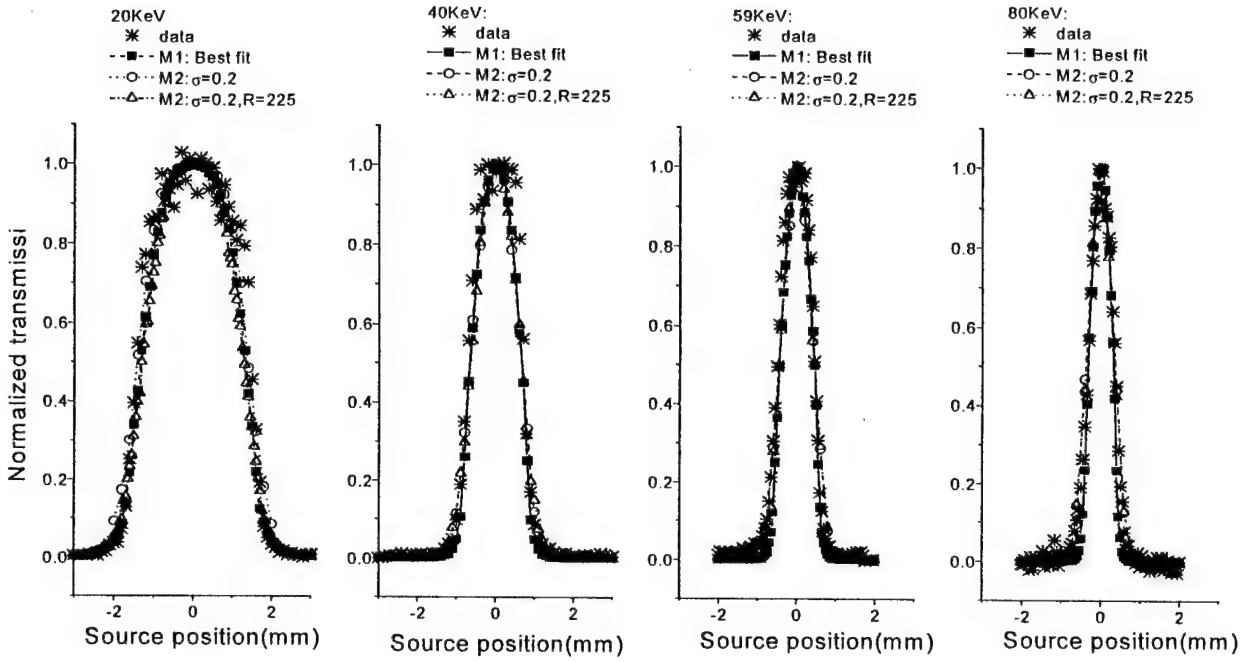

Figure 15 Simulated source scan curves using M1 and M2 compared with experimental data at four different photon energies. They all fit the data quite well. For M2, this figure also verifies that the bending has no visible effect on the source scan. The best-fit parameters for M1 are R = 125 m, $\Delta\theta_{max}$ = 0.35 mrad, s = 6 μm and z = 0.5 nm.

2.E.4 Best-fits of all the fibers and analysis of the results

Using the algorithm described above, the best-fit parameters of M2 for Fiber A, D and E were obtained. The best-fit parameters for both M1 and M2 are shown in Table 1. The best-fit curves of M1 and M2 along with the experimental data are shown in Figures 16-18. The fibers are described in *Table 1.*

In Figure 17, the transmission for fiber A shows a rapid drop for energies above 30 keV. Although fiber D has lower fractional open area than fiber A, its transmission exceeds that of fiber A at energies above 30 keV. This is because fiber A is thin (0.5 mm in outer diameter) and flexible, therefore difficult to keep straight in the measurement apparatus. Model M2, which can vary only bending and waviness, requires a much sharper bend for fiber A than for fi-

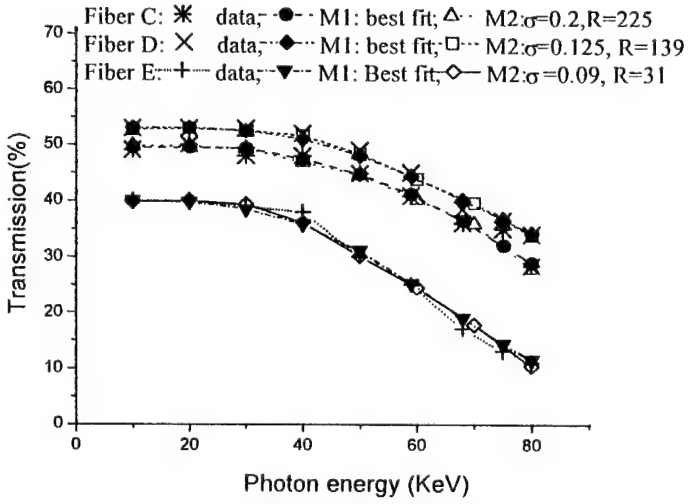

Figure 16. Simulations of transmission spectra of fiber C, fiber D and fiber E with their best-fit parameters compared with the experimental data. All parameters related to this figure are listed in Table 1.

ber D. This bending is more significant at high energies, where the critical angles are smaller.

Transmission curves for fiber C and D are similar in shape and are nearly flat up to 60 keV, as shown in figure 15. However, the smaller channel size for fiber D results in the simulation being less sensitive to bending. Therefore a larger bending curvature (smaller radius) is required for fiber D. The waviness correction for fiber D must therefore be smaller to keep the transmission about the same as for fiber C.

Fiber E is the thinnest fiber. Table 1 shows that it has the largest bending correction because of its flexibility. Its transmission curve is flat up to 40 keV. This is due to its very small channel size, as discussed in the comparison of fiber C and fiber D. However, if the channel size is too small, as in fiber E, it also results in more reflections being needed for a photon to traverse the fiber and may have introduced other defects such as blocked channels. This is why the transmission is only 40% for the energies below 40 keV although the open area is around 55%.

The high transmission and the simulation results show that the quality of the capillary fibers is quite good. The bending radius is above 130 meters for type 3 and type 4 capillaries. It is hopeful that we can further improve the high-energy transmission performance of polycapillary fibers by decreasing to an optimum channel size, and making them more rigid.

Because Model M2 is physically plausible, gives reasonable results, and matches the experimental data very well, as shown in figures 16 and 17, we can use it to simulate other polycapillary optics. Compared to M1, which uses four parameters, M2 uses only two parameters, which makes simulating the experimental results more straightforward, easier and timesaving. In addition, roughness does not have much effect in the energy range 10-80 keV, so M2 gives us more confidence with fewer parameters.

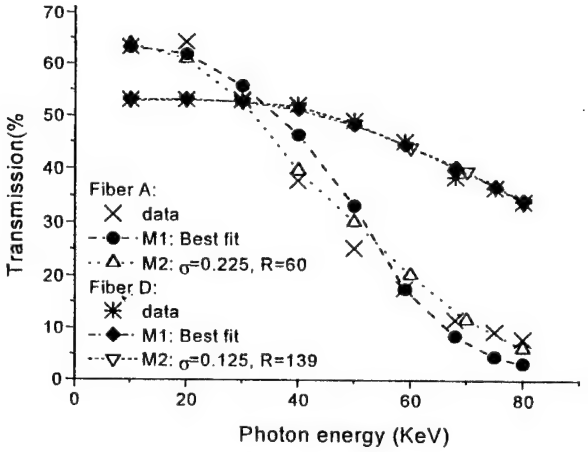

Figure 17. Simulations of transmission spectra of fiber A and fiber D with their best-fit parameters compared with the experimental data. All parameters related to this figure are listed in Table 1.

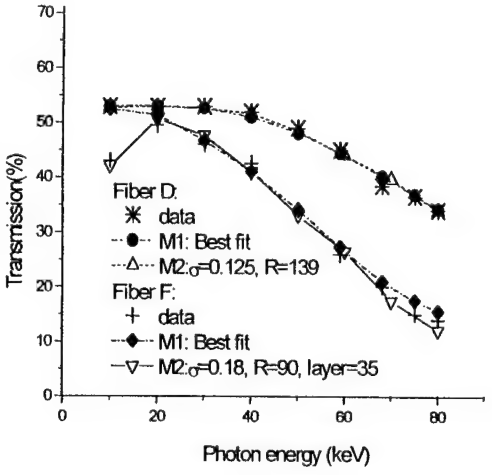

Figure 18. Simulations of transmission spectra of fiber D (unexposed) and fiber F (exposed) with their best-fit parameters compared with the experimental data. Layer = 35 means that there is a 35 micron glass layer added. All parameters related to this figure are listed in Table 1 except the glass layer.

2.E.5 An analysis of a radiation-damaged fiber

The measured transmission spectra and source scans provide sensitive tools for analyzing capillary quality. This method was used to analyze the effect of radiation damage on fiber F that has the same type and same length as fiber D. Radiation damage has been

observed after a very large dose of x-ray exposure.[12] It was found that prolonged exposure to synchrotron white beam radiation could cause a measurable bend for a thin fiber. This bending can be reduced by annealing and by holding the fiber rigid during exposure. Fiber F had 1.8 MJ/cm^2 exposure before the current measurements. There is no visually observable bending or other visible damage.

The transmission spectrum and its simulation for fiber F are compared with an unexposed capillary of the same type, fiber D, in Figure 16. The measured data shows a significant transmission drop above 30 keV and below 10 keV. The simulation indicates that the exposed capillary has more bending and waviness. The bending radius was changed from 139 m to 90 m and the waviness σ changed from 0.125 mrad to 0.18 mrad. Although these profile changes have a significant effect the transmission, they are still very small and not visible. The transmission drop below 20 keV can be explained by adding 35 μm x-ray-absorbing glass layer as shown in Figure 18.[13]

2.F Measurement and analysis of leaded glass fibers

As discussed in the previous section, the geometric simulation model M_2 has been used to analyze the experimental data for number of borosilicate single capillaries. The analysis shows that the simulation results fit fairly will with the experimental data.

In this section, we will analyze the experimental results of a number of leaded glass single capillaries using model M_2. Leaded glass polycapillary optics could be a candidate for scatter rejection because of lead's superior absorption. Lead glass optics could be shorter and therefore easier to manufacture. Lead glass optics may be the fast way to be bring capillary optics to clinical use. Transmission of a leaded glass polycapillary in the 9-80 keV energy range is shown in figure 19. The description of these capillaries and the simulation parameters listed in table II. The characteristic of the transmission spectra leaded glass fiber are similar to the radiation-damaged borosilicate fiber, i.e, the transmission drops off at both lower energies and higher energies, as shown in figure 19. In addition to the waviness and bending simulation parameters, the simulation has to include a leaded glass layer of 50 μm thick or less, to fit the experimental data.

Table II. Fiber description

					Model M2					Model M2		
Fiber #	Outer diameter	Channel size μm	Open area %	Length mm	s μm	R m	W mrad	Z nm	Layer μm	R m	W mrad	Layer μm
A	0.54	12	60	60	6	33	0.5	2	50	42.5	0.3	54
B1	0.51	12	60	60	6	52.5	0.3	2	30	59	0.205	26
B2	0.51	12	60	30	6	30	0.3	2	35	30	0.205	37.5
C	0.54	11	50	60	6	28	0.5	2.25	30	27.5	0.26	37

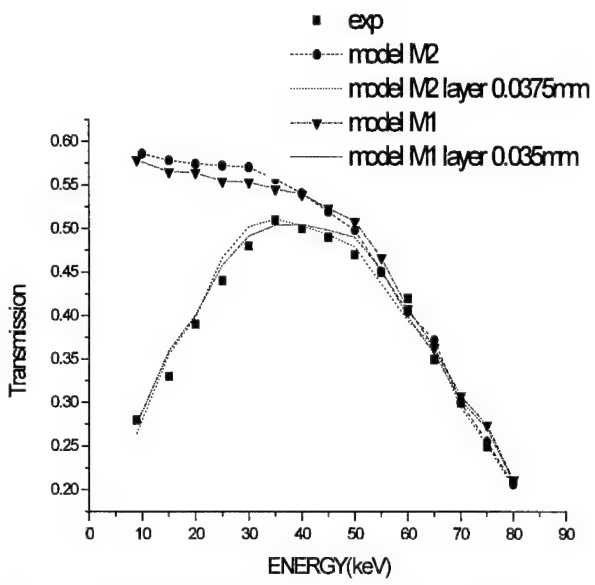

Figure 19. Simulated transmission spectra using model M1 and M2 for leaded glass single fiber type B1of length 60 mm compared to the experimental data.

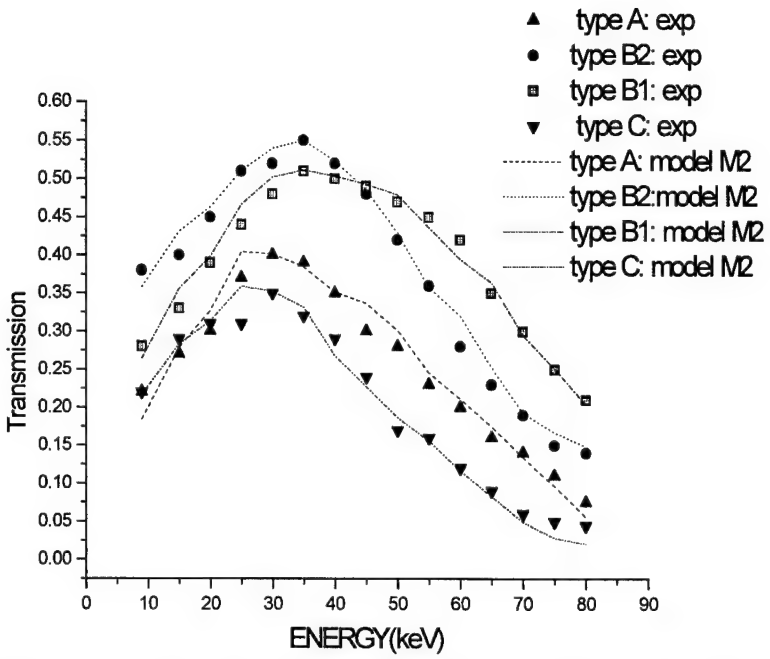

Figure 20. Simulated transmission spectra using model M2 for leaded glass single fiber A, fiber B and fiber C. All parameters compared with experiment data and related to this figure are listed in table II.

Figure 19 shows that both simulations model M_1 and model M_2, fit fairly well with the transmission

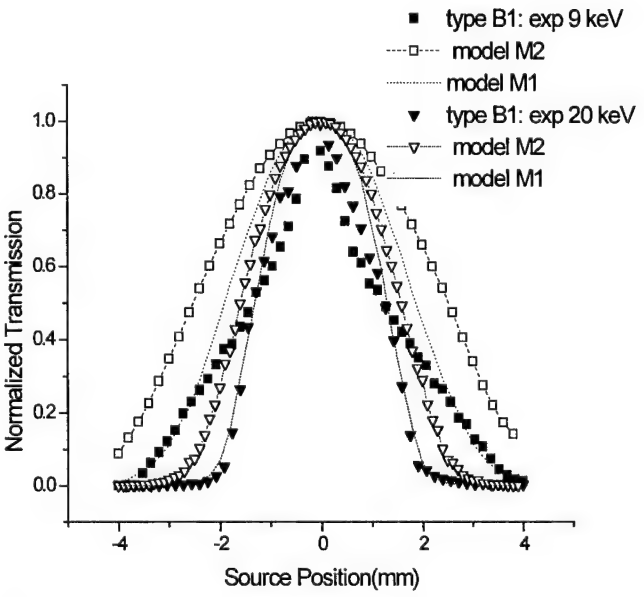

Figure 21. Simulations of source scan curve using model M1 and M2 compared with experiment data for leaded glass for single fiber.

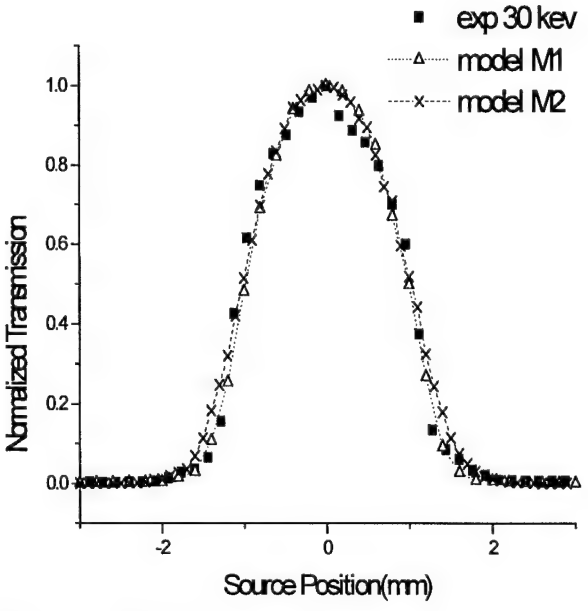

Figure 22. Simulation of source scan curves using model M1and M2 compared with experimental data for leaded glass for type B1.

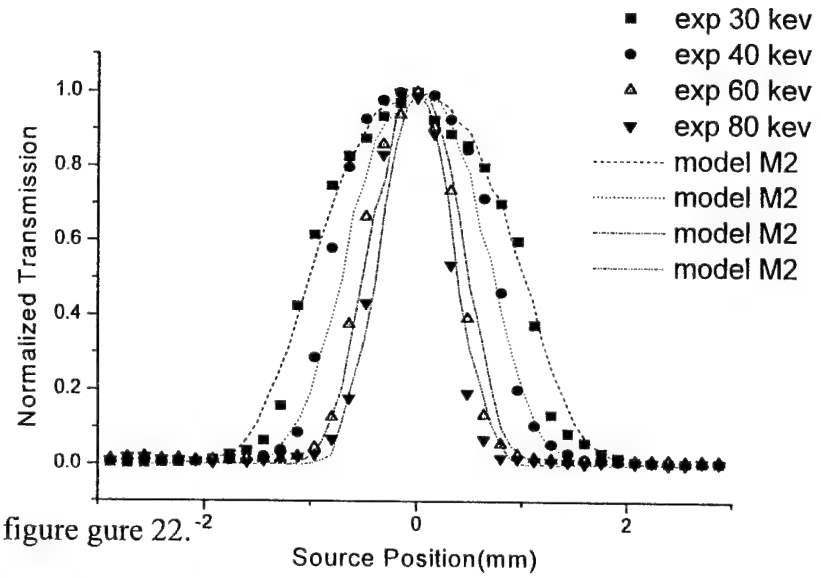

figure gure 22.

Figure 23. Simulation of source scan curves using model M2 compared with experimental data at four energies for type B1.

spectrum for the type B1 fiber once a layer of leaded glass is added.. Since model M2 does not include the surface roughness and leaded glass fibers have very high roughness, it is expected that model M2 does not fit the source scan data well at energy 20 keV as well as model M1, as shown in figure 21. Neither model fits the data well at 9keV However, model M_2 fits the source scan data fairly well at higher energies, as shown in figure 22.

Finally, the measured transmission spectra for a number of leaded glass fibers II are shown in figure 20.

The models fit the transmission spectra fairly well, with the parameters listed in table II.

2G. Measurement of the transmission, output divergence, and uniformity of collimating lens.

This collimating lens is 3 cm x 3 cm on the parallel end, and 2.9 cm x 2.9 cm on the focusing end. The focal length of the lens was determined by measuring the transmission at various distances from the source. The highest transmission determines the focal distance, which was found to be 193 cm for this lens, as shown in figure 27.

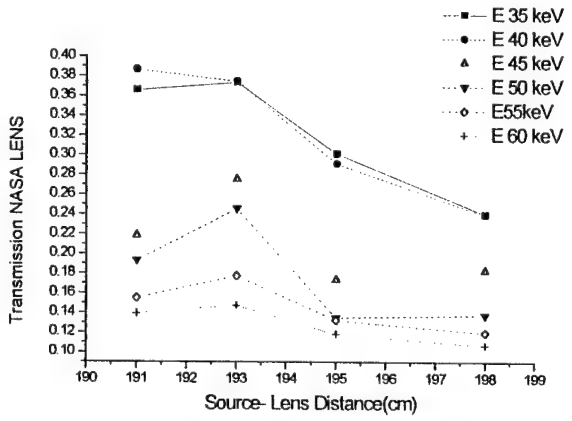

Figure 27. The transmission as function of source–lens distance at various energies for new collimating lens with focal distance of 193 cm.

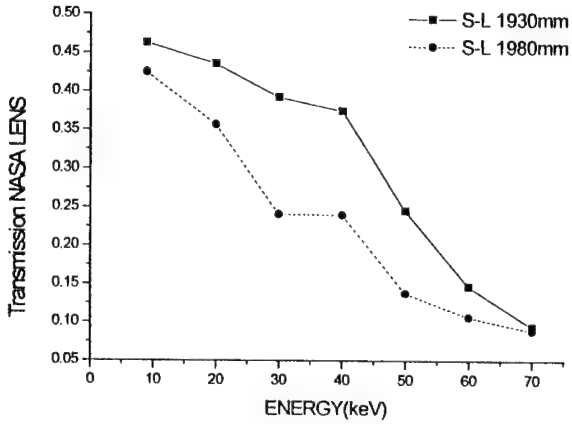

Figure 28. The measured transmission vs energy at 193 cm and 198 cm source-lens distances.

The transmission of this lens was measured by placing the source at focal distance. Figure 28 shows that this lens has transmission close to 45 % at 20 keV.

To measure the output divergence of this lens, a high quality single crystal (100) silicon wafer is placed between the exit end and the detector. The output divergence of this lens is less than 6 mrad as shown in figure 29.

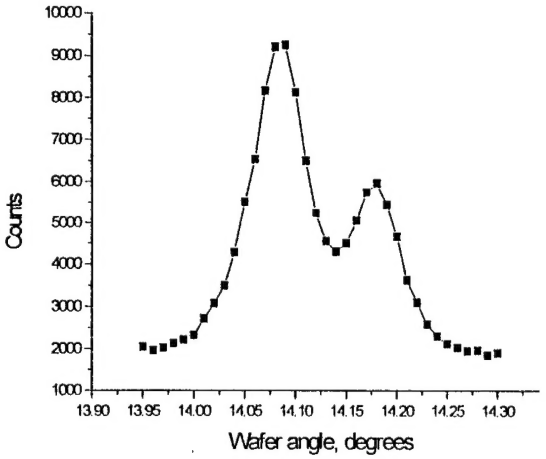

Figure 29. Output divergence of collimating lens, measured by rocking a silicon crystal in the beam

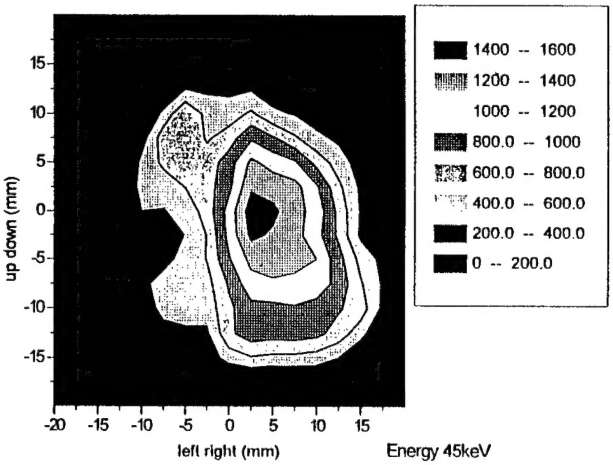

Figure 30. Output intensity distributions for new collimating lens at 198 cm source –lens distance.

The uniformity of the lens was measured by placing an aperture in front of the lens and taking aperture scans with the source, lens, and the detector are fixed. Surface area plots of the intensity as a function of aperture position can be seen in figure 30.

2.H Measurement of a prototype post-patient monolithic optic

Polycapillary optics can be manufactured either as monolithic optics, shaped from a single large fiber, or as multi fiber optics, with multiple fibers strung through grids. Although a lot of progress has been made on manufacture of monolithic optics, there are still technological difficulties in producing good quality large scale monolithic so far. However, magnification, with resulting enhancement requires monolithic optics.

In this section transmission measurements for lens J as prototype monolithic optic, are presented. The basic geometric of this post patient monolithic optic were measured as following:
Length of the optic =129 mm
Output diameter=8.25 mm
Input diameter=6.1 mm
Channel size=25 μm
Focal distance=500 mm
The x-ray generator used in the experiment is a low current microfocus MS50 with a 50 μm spot size, tungsten target, and a maximum operating voltage of 100 kVp. Because of its high background scattered x-rays, this source is enclosed in 6mm thick lead box and therefore the source can not be moved in z direction. The optic to the source distance was then changed by moving the optic in the z direction.

Variation of acceptance angle of the optics as a function of source optic distance was used primarily to determine both focal distance of prototype monolithic optic and the input depth field. The acceptance angle is the full width of the source scan divided by the source to optic distance. The acceptance angle is a minimum at the focal distance, where the transmission is maximized. Focal distance of this optic was determined by moving the source in x and y direction to maximize the transmission at certain position of the optic.

Figure 24 shows that the focal length and the input depth filed of this optic are 500 mm and 20 mm, respectively. This measured focal length is in good agreement with focal length determined using the transmission as function of source –optic distance curve as shown in figure 24. Finally the transmission efficiency of this fiber was measured at the focal point. This optic is fairly good since its transmission efficiency is 20.8 % at 20 keV, 18 % at 23 keV and 16.33 % at 25 keV. At mammographic energy (20 keV) the high angle transmission of this optic close to zero as shown in figure 26.

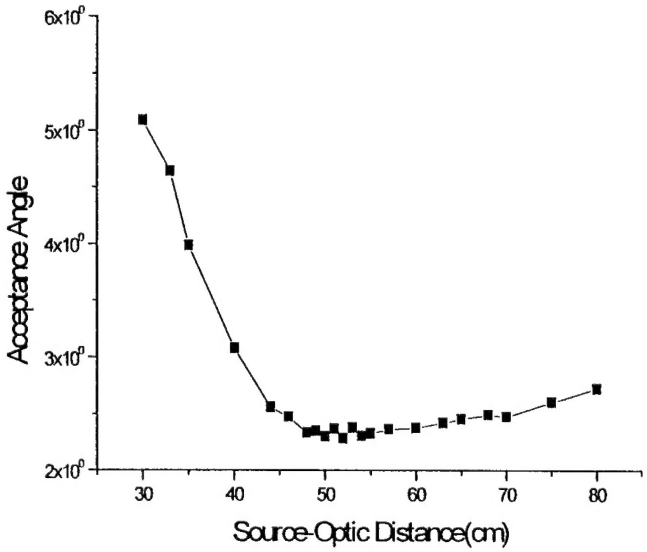

Figure 24. Measured acceptance angle as function of source-optic distance for optic J at 20 keV

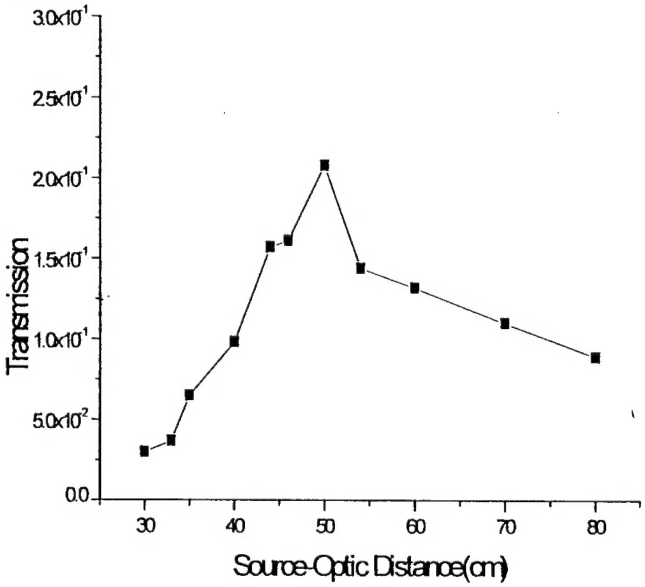

Figure 25. Measured transmission vs source –optic distance of optic J at 20 keV.

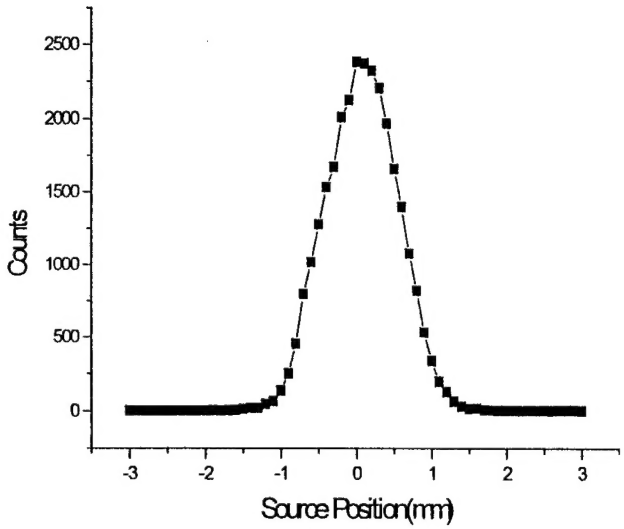

Figure 26. Measured of scan source for optic J at focal distance.

3. Conclusion

A new, more physical model for describing profile defects in polycapillary x-ray optics at high energies for mammography has been developed. The simulation model M2, a geometric simulation with waviness and bending correction, is physically plausible and works quite well in explaining the transmission spectra. It uses only two parameters, which makes simulating the experimental results and designing lenses straightforward, easy and timesaving. According to the simulations, waviness and bending in the capillary channel profiles can be particularly harmful for high-energy photons because of the smaller critical angle at high energies. Roughness is not important in the simulation. It is expected that increasing the rigidity and straightness of the fiber and reducing the channel size to an optimum value can further increase the transmission. The spectra of transmission versus energy have been found to be a very sensitive tool in capillary quality analysis, and transmission versus source scan curve measurements can also provide significant information. Lead glass shows promise in allowing for shorter, higher transmission optics which will easier to manufacture. The new collimating lens with long focal distance of around 2 m has good transmission and uniformity.

3. References

[1] ACS(American Cancer Society) "Cancer Facts And Figures," Atlanta, , GA: American Cancer Society, 1993.
[1] P. Strax, "Detection Of Breast Cancer," Cancer 66,1336-1340, supplement,(1990).
[1] M. A. Kumakhov, F. F. Komarov, "Multiple Reflection from Surface X-ray Optics", Physics Reports, 191,(5):p. 289-350,1990.
[1] C. A. MacDonald, etc., "Quantitative measurements of the Performance of Capillary X-ray Optics "Multi-layer and Grazing Incidence X-Ray/EUV optics II, R. B. Hoover and A. Walker, eds., SPIE Proc. vol. 2011, 1993.
[1] J. B. Ullrich, V. Kovantsev, C. A. MacDonald, "Measurements of Polycapillary X-ray Optics," Jour. Appl. Phys., 74(10),Nov. 15.,1993.
[1] C.A. MacDonald, "Applications and Measurements of Polycapillary X-Ray Optics" Journal of X-ray Science and Technology, Special issue for the proceedings of the Monochromatic X-ray Workshop, 1993.
[1] C.C. Abreu, D. G. Kruger, C.A. MacDonald, C.A. Mistretta, W.W. Peppler, Q. F. Xiao, Measurements of Capillary X-ray Optics with Potential for use in Mammographic Imaging, Medical Physics.
[1] Q. F. Xiao, I. Y. Ponamarev, A. I. Kolomitsev and J.C. Kimball, "Numerical simulations for capillary-based x-ray optics," in X-Ray Detector Physics and Applications, R. B. Hoover, ed., SPIE 1992.
[1] B. L. Henke, E. M. Gullikson, and J.C. Davis, Atomic Data and Nuclear Data Tables, 54 (2), p. 181, 1993.
[1] J. C. Kimball, D. Bittel, "Surface roughness and scattering of glancing angle x-rays: Application to x-ray lenses", Jour. Appl. phys. 74 (2), 15 July 1993, pp. 877-883.
[1] Lei Wang, B. K. Rath, W. M. Gibson, J.C. Kimball, C.A. MacDonald, "Performance Study of Polycapillary Optic Performance for Hard X rays," Journal of Applied Physics, 80 (7), pp.3628-3638, October 1, 1996.

[1] B. K. Rath, D. C. Aloisi, D. H. Bilderback, N. Gao, W. M. Gibson, F. A. Hofmann, B. E. Homan, C. J. Jezewski, I. L. Klotzko, J. M. Mitchell, S. M. Owens, J. B. Ullrich, Lei Wang, G. M. Wells, Q. Xiao, C. A. MacDonald, "Effects of intense x-ray radiation on polycapillary fiber performance", in SPIE vol. 2519, X-Ray and Ultraviolet Sensors and Application, 1995.

[1] B. K. Rath, Lei Wang, B. E. Homan, F. Hofmann, W. M. Gibson, C. A. MacDonald, "Measurements and analysis of Radiation effects in polycapillary x-ray optics", J. Appl. Phys.